

A CANDIDATE $Z \sim 10$ GALAXY STRONGLY LENSED INTO A SPATIALLY RESOLVED ARC

BRETT SALMON^{1,†}, DAN COE¹, LARRY BRADLEY¹, MARUSA BRADAČ², KUANG-HAN HUANG², VICTORIA STRAIT², PASCAL OESCH³, RACHEL PATERNO-MAHLER⁴, ADI ZITRIN⁵, ANA ACEBRON⁵, NATHÁLIA CIBIRKA⁵, SHOTARO KIKUCHIHARA^{6,7}, MASAMUNE OGURI^{7,8,9}, GABRIEL B. BRAMMER¹, KEREN SHARON⁴, MICHELE TRENTI¹⁰, ROBERTO J. AVILA¹, SARA OGAZ¹, FELIPE ANDRADE-SANTOS¹¹, DANIELA CARRASCO¹⁰, CATHERINE CERNY⁴, WILLIAM DAWSON¹², BRENDA L. FRYE¹³, AUSTIN HOAG², CHRISTINE JONES¹¹, RAMESH MAINALI¹³, MASAMI OUCHI^{6,8}, STEVEN A. RODNEY¹⁴, DANIEL STARK¹³, KEIICHI UMETSU¹⁵

¹Space Telescope Science Institute, Baltimore, MD, USA

²Department of Physics, University of California, Davis, CA 95616, USA

³Geneva Observatory, University of Geneva, Ch. des Maillettes 51, 1290 Versoix, Switzerland

⁴Department of Astronomy, University of Michigan, 1085 South University Ave, Ann Arbor, MI 48109, USA

⁵Physics Department, Ben-Gurion University of the Negev, P.O. Box 653, Beer-Sheva 84105, Israel

⁶Institute for Cosmic Ray Research, The University of Tokyo, 5-1-5 Kashiwanoha, Kashiwa, Chiba 277-8582, Japan

⁷Department of Physics, Graduate School of Science, The University of Tokyo, 7-3-1 Hongo, Bunkyo-ku, Tokyo 113-0033, Japan

⁸Kavli Institute for the Physics and Mathematics of the Universe (Kavli IPMU, WPI), University of Tokyo, Chiba 277-8582, Japan

⁹Research Center for the Early Universe, The University of Tokyo, 7-3-1 Hongo, Bunkyo-ku, Tokyo 113-0033, Japan

¹⁰School of Physics, University of Melbourne, VIC 3010, Australia

¹¹Harvard-Smithsonian Center for Astrophysics, 60 Garden Street, Cambridge, MA 02138, USA

¹²Lawrence Livermore National Laboratory, P.O. Box 808 L- 210, Livermore, CA, 94551, USA

¹³Department of Astronomy, Steward Observatory, University of Arizona, 933 North Cherry Avenue, Rm N204, Tucson, AZ, 85721, USA

¹⁴Department of Physics and Astronomy, University of South Carolina, 712 Main St., Columbia, SC 29208, USA

¹⁵Institute of Astronomy and Astrophysics, Academia Sinica, PO Box 23-141, Taipei 10617, Taiwan

Submitted to *ApJL* on 1/9/17

ABSTRACT

The most distant galaxies known are at $z \sim 10 - 11$, observed 400 – 500 Myr after the Big Bang. The few $z \sim 10 - 11$ candidates discovered to date have been exceptionally small—barely resolved, if at all, by the *Hubble Space Telescope*. Here we present the discovery of SPT0615-JD, a fortuitous $z \sim 10$ ($z_{\text{phot}} = 9.9 \pm 0.6$) galaxy candidate stretched into an arc over $\sim 2.5''$ by the effects of strong gravitational lensing. Discovered in the Reionization Lensing Cluster Survey (RELICS) *Hubble* Treasury program and companion S-RELICS *Spitzer* program, this candidate has a lensed H -band magnitude of 25.7 ± 0.1 AB mag. With a magnification of $\mu \sim 4 - 7$ estimated from our lens models, the de-lensed intrinsic magnitude is 27.6 ± 0.3 AB mag, and the half-light radius is $r_e < 0.8$ kpc, both consistent with other $z > 9$ candidates. The inferred stellar mass ($\log[M_*/M_\odot] = 9.7^{+0.7}_{-0.5}$) and star formation rate ($\log[\text{SFR}/M_\odot \text{ yr}^{-1}] = 1.3^{+0.2}_{-0.3}$) indicate that this candidate is a typical star-forming galaxy on the $z > 6$ SFR– M_* relation. We note that three independent lens models predict two counterimages, at least one of which should be of a similar magnitude to the arc, but these counterimages are not yet detected. Counterimages would not be expected if the arc were at lower redshift. However, the only spectral energy distributions capable of fitting the *Hubble* and *Spitzer* photometry well at lower redshifts require unphysical combinations of $z \sim 2$ galaxy properties. The unprecedented lensed size of this $z \sim 10$ candidate offers the potential for the *James Webb Space Telescope* to study the geometric and kinematic properties of a galaxy observed 500 Myr after the Big Bang.

1. INTRODUCTION

With its high resolution and sensitivity, observations using the *Hubble Space Telescope* (*HST*) have sharpened our understanding of the high- z universe. Deep and wide extragalactic imaging surveys with ACS and WFC3 have uncovered thousands of galaxies at $z > 6$ in blank fields (see Finkelstein 2016; Stark 2016, for reviews), including the most distant galaxy found to-date at $z = 11.1$ (GN-z11; Oesch et al. 2016). In addition, we have prioritized *HST* to observe the most massive galaxy clusters, taking advantage of the natural telescopes they create via strong gravitational lensing (CLASH, PI Postman; Frontier Fields, PI Lotz; RELICS, PI Coe). This investment in lensing fields has proven fruitful. We have discovered highly magnified (MACS1149-JD, Zheng et al. 2012; Hoag et al. 2017; MACS1115-JD and MACS1720-JD,

Bouwens et al. 2014; MACS0416-JD, Infante et al. 2015) and multiply-imaged galaxies (MACS0647-JD, Coe et al. 2013; A2744-JD, Zitrin et al. 2014) at redshifts up to $z \sim 10.8$, which have allowed us to study faint UV metal lines (Stark et al. 2014; Rigby et al. 2015; Mainali et al. 2017), nebular emission lines (Smit et al. 2017; Stark et al. 2015; Hoag et al. 2017; Laporte et al. 2017), and the star formation rate density deep into the epoch of reionization (Oesch et al. 2014, 2017).

However, little is known in detail about the $z > 9$ universe, and the handful of candidates found so far exhibit peculiar properties. At $z \sim 11$, MACS0647-JD has a radius smaller than 100 pc, the size of Giant Molecular Clouds in the local universe. GN-z11 is three times brighter than the characteristic UV luminosity (L_*) of galaxies at that distance, surprisingly bright given the CANDELS search area. Both $z \sim 10$ candidates MACS1149-JD and M0416-JD appear to have

† bsalmon@stsci.edu

an evolved stellar population of ≈ 340 Myr (due to red $[3.6 \mu\text{m}]-[4.5 \mu\text{m}]$ *Spitzer* colors), when the age of the universe was only ≈ 500 Myr (Hoag et al. 2017). *JWST* NIRC*am* will better sample the rest-frame UV-to-optical colors which will break some parameter degeneracies and challenge these initial inferences. However, with typical $z \sim 10$ effective radii of $< 0.2''$ and a NIRC*am* PSF FWHM² of $\sim 0.05''$ at $1.5 \mu\text{m}$, it will still be difficult to resolve these galaxies spatially. Ideally, we can use the help of strong lensing to study the kinematics and intrinsic stellar populations at $z \sim 10$ in detail.

In this Letter we present a galaxy gravitationally lensed into an arc with a photometric redshift of $z_{\text{phot}} = 9.9 \pm 0.6$. Discovered in the Reionization Lensing Cluster Survey (RELICS) *Hubble* (*HST*) and *Spitzer Space Telescope* imaging, the arc features of this candidate extend across $\sim 2.5''$, allowing unprecedented physical resolution deep in the epoch of reionization. This new candidate has an *HST* F160W *H*-band magnitude of $H = 25.7 \pm 0.1$ AB, bright enough for follow-up spectroscopic or grism observations. In this work, we present the supporting evidence that this candidate is indeed at $z \sim 10$, and discuss the remaining uncertainties. Throughout, we assume concordance cosmology with $H_0 = 70 \text{ km s}^{-1} \text{ Mpc}^{-1}$, $\Omega_{\Lambda,0} = 0.7$ and $\Omega_{\text{M},0} = 0.3$.

2. DATA AND PHOTOMETRY

The galaxy cluster SPT-CL J0615-5746 (hereafter SPT0615-57; also known as PLCK G266.6-27.3) was discovered independently by the South Pole Telescope survey (Williamson et al. 2011) and the Planck Collaboration et al. (2011). It is exceptionally massive ($M_{500} = 6.8 \times 10^{12} M_{\odot}$) for its high redshift ($z = 0.972$). The SPT and Planck teams obtained *HST* imaging (GO 12477 and 12757) of the cluster with the ACS/WFC F606W filter *V* (1-orbit depth) and F814W filter *I* (combined 2-orbit depth). RELICS (GO 14096) obtained ACS/WFC imaging (1 orbit) in F435W *B* and WFC3/IR imaging (2 orbits) in F105W *Y*, F125W *J*, F140W *JH*, and F160W *H*.

RELICS obtained similar *HST* imaging with WFC3/IR and ACS as needed on a total of 41 clusters. The details of the image reduction, SExtractor (version 2.8.6; Bertin & Arnouts 1996) object selection, and *HST* photometry are described by Salmon et al. (2017) and Coe et al. (in prep). SPT0615-57 was the second highest high- z -producing cluster field out of the 41 RELICS fields, revealing 25 new candidate galaxies over the redshift range $5.5 < z < 8.5$ (Salmon et al. 2017).

Table 1 shows the three $z > 9$ candidates found in RELICS after fitting photometric redshifts to only *HST* data. We then vetted these candidates by checking *Spitzer* data from the S-RELICS programs (PI Bradać; PI Soifer). The IRAC channel 1 and 2 bands ($3.6 \mu\text{m}$ and $4.5 \mu\text{m}$ respectively, with ≈ 5 -hour depth per band), correspond to rest-frame optical flux at $z \sim 9 - 10$ and are invaluable for distinguishing between intrinsically bluer $z \sim 10$ star-forming galaxies and intrinsically redder $z \sim 3$ interloper galaxies. The *Spitzer* fluxes were extracted using T-PHOT (Merlin et al. 2016) which uses the

TABLE 1
RELICS $z \sim 10$ CANDIDATE AND $z \sim 3$ INTERLOPERS

Field	SPT0615-57	PLCKG138-10	RXC0018+16
RELICS ID	336	748	1107
α_{J2000}	06:15:55.03	02:27:00.86	00:18:33.84
δ_{J2000}	-57:46:19.56	49:00:22.68	16:25:18.84
B_{435}	> 28.7	> 26.8	> 28.8
V_{606}	> 28.4	> 28.4	> 28.8
I_{814}	> 29.5	> 27.0	> 29.4
Y_{105}	> 27.3	> 27.3	> 28.4
J_{125}	> 26.5	> 26.5	> 26.9
JH_{140}	> 26.3	26.0 ± 0.2	> 26.6
H_{160}	25.7 ± 0.1	25.2 ± 0.1	26.1 ± 0.1
[3.6 μm]	25.2 ± 0.3	23.4 ± 0.1	23.1 ± 0.1
[4.5 μm]	24.4 ± 0.3	22.9 ± 0.1	22.8 ± 0.1
$z_{\text{phot},HST}$ only ^a	$9.6^{+0.7}_{-7.4}$	$10.0^{+0.6}_{-7.5}$	$9.9^{+0.7}_{-1.0}$
$z_{\text{phot},HST+Spitzer}$	$9.9^{+0.6}_{-0.6}$	$2.7^{+0.1}_{-0.1}$	$3.6^{+0.2}_{-0.2}$

Notes: ^aPhotometric redshifts found using BPZ. The two $z \sim 3$ interlopers from PLCKG138-10 and RXC0018+16 were initially identified as $z \sim 10$ candidates prior to including the *Spitzer* data, whereas the candidate in SPT0615-57 remained at $z \sim 10$.

higher-resolution *HST* imaging as a prior to extract photometry from the lower resolution *Spitzer* images. First, we produce PSF convolution kernels based on all available *HST* images. We manually sharpen the PSF to minimize residuals between the convolved image and the *Spitzer* images. Then, we run T-PHOT on the entire cluster field to extract the *Spitzer* photometry.

After obtaining the *Spitzer* photometry and re-running the photometric redshifts, we rule out two candidates as low- z interlopers, leaving one $z \sim 10$ candidate. Fig. 1 shows image cutouts of this candidate, hereafter named SPT0615-JD (“JD” for *HST* F125W *J*-band dropout), in each of the available *HST* and *Spitzer* bands, as well as a WFC3/IR color composite. SPT0615-JD has an AB magnitude of 25.7 ± 0.1 in F160W detected with $S/N \sim 11$ (the F160W exposures were in two epochs 44 days apart and each detected the source with $S/N \sim 5$). The extended arc shape is consistent with the direction of lensing shear expected from the cluster (see §3). The bands blueward of F140W are undetected with $S/N \lesssim 2$, and F140W is just undetected ($S/N = 2.9$). Importantly, we emphasize that observed-frame size of SPT0615-JD is rather large ($\sim 2.5''$ long), and can easily be spatially resolved by *JWST* (see §5).

We note that these image cutouts reveal an important caveat to the *Spitzer* fluxes of SPT0615-JD. T-PHOT reports a maximum covariance between SPT0615-JD and all other sources fit simultaneously (max CV ratio) of ~ 1.4 for both the $3.6 \mu\text{m}$ and $4.5 \mu\text{m}$ images. This implies a covariance between the *Spitzer* photometry of SPT0615-JD and a nearby source. The $8'' \times 8''$ *HST* image in Fig. 1 shows an IR-bright nearby $z \sim 3$ galaxy. We conclude that the *Spitzer* fluxes for SPT0615-JD are biased by this source and are likely over-estimated. Even so, the fluxes in each *Spitzer* band are already several magnitudes fainter than typical low- z interlopers. This is critical because while all $z \sim 10$ solutions could have lower *Spitzer* fluxes, the $z \sim 2$ solution requires them to be high, especially at $4.5 \mu\text{m}$. As we will discuss in §4,

² see <https://jwst-docs.stsci.edu>

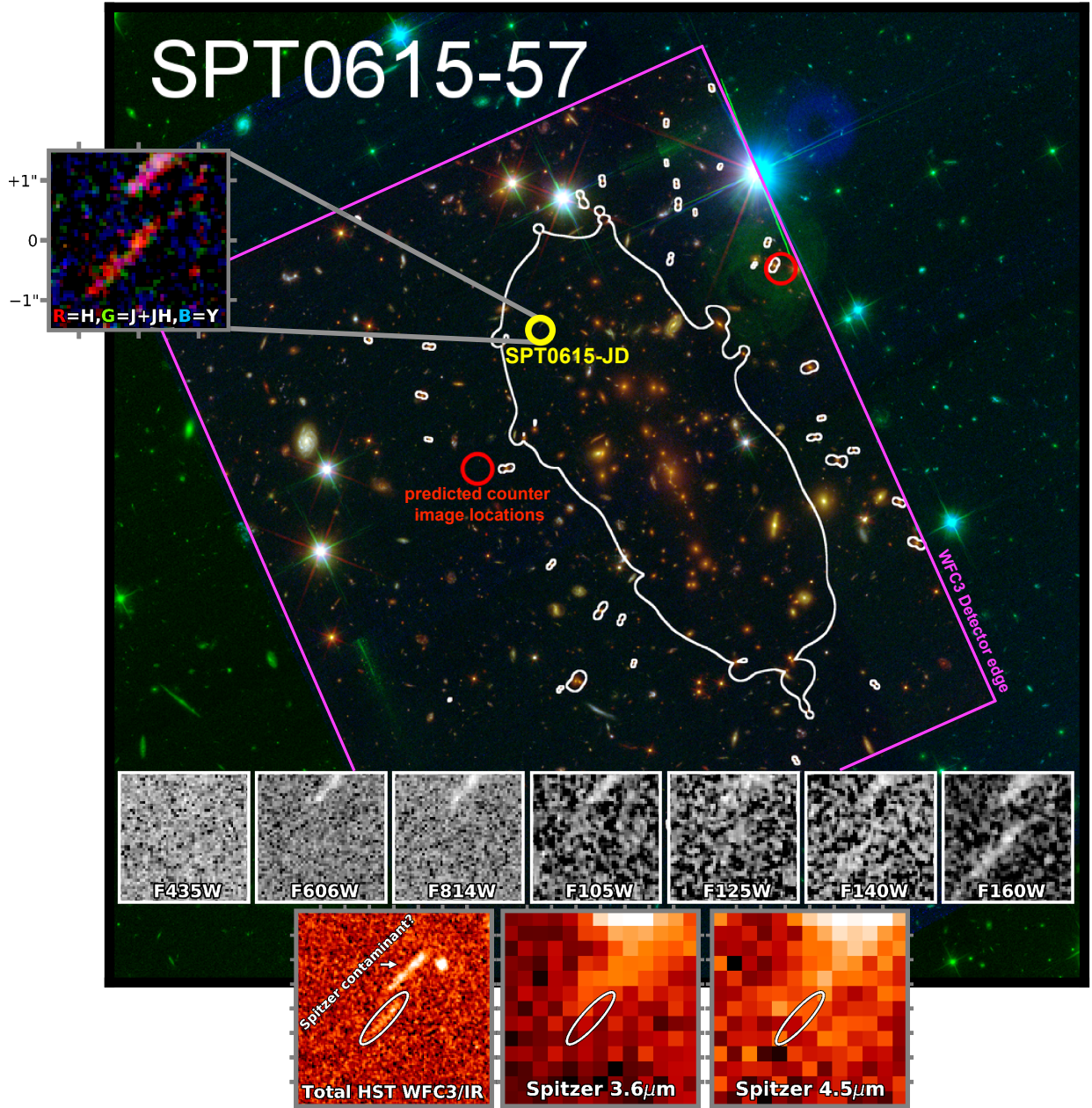


FIG. 1.— A $3'25 \times 3'25$ color image of the *HST* RELICS cluster field SPT0615-57. The yellow circle marks the location of the $z \sim 10$ candidate SPT0615-JD. The white lines and red circles show the lens-model $z = 10$ critical curves and predicted locations of the yet undetected counterimages. The violet lines mark the edge where WFC3/IR data is available. The expanded inset is a $3'' \times 3''$ WFC3/IR RGB color image with the R channel as F160W, G as the sum of F125W and F140W, and B as F105W. The bottom row of insets are the ACS images followed by WFC3/IR images, all $3'' \times 3''$ and 60 mas resolution. The candidate is missing in the bands blueward of F140W, indicating a strong spectral break. Bottom row: larger $8'' \times 8''$ cutouts with ellipses marking the position of SPT0615-JD. Bottom left, right, and middle: A weighted stack of all four WFC3/IR bands centered on SPT0615-JD, and the *Spitzer* $3.6 \mu\text{m}$ and $4.5 \mu\text{m}$ images. The *Spitzer* flux from the nearby bright $z \sim 3$ galaxy crowds the $z \sim 10$ candidate, which appears otherwise faint.

the inflated *Spitzer* fluxes also increase the inferred $z \sim 10$ UV dust attenuation, which should be considered an upper limit. Upcoming deeper *Spitzer* imaging (PI Bradač) of this cluster will improve constraints on the flux and derived properties of this candidate.

3. LENS MODELS

We identify three sets of multiply-imaged galaxies: two with spectroscopic redshifts ($z = 1.358$ and $z = 4.013$) and one whose redshift is free to vary in the modeling. (Paterno-Mahler et al., in preparation). Based on these,

we produce three lens models using Lenstool (Jullo et al. 2007), GLAFIC (Oguri 2010), and the Zitrin et al. (2015) Light Traces Mass (LTM) method. Based on these models, we estimate the magnification of SPT0615-JD to be $\mu \sim 4 - 7$.

All three models predict two counterimages at the positions shown in Fig. 1. Our results using GLAFIC (Kikuchihara et al., in preparation) and Lenstool (Paterno-Mahler et al., in preparation) predict the upper-right counterimage is ≈ 1 magnitude fainter than

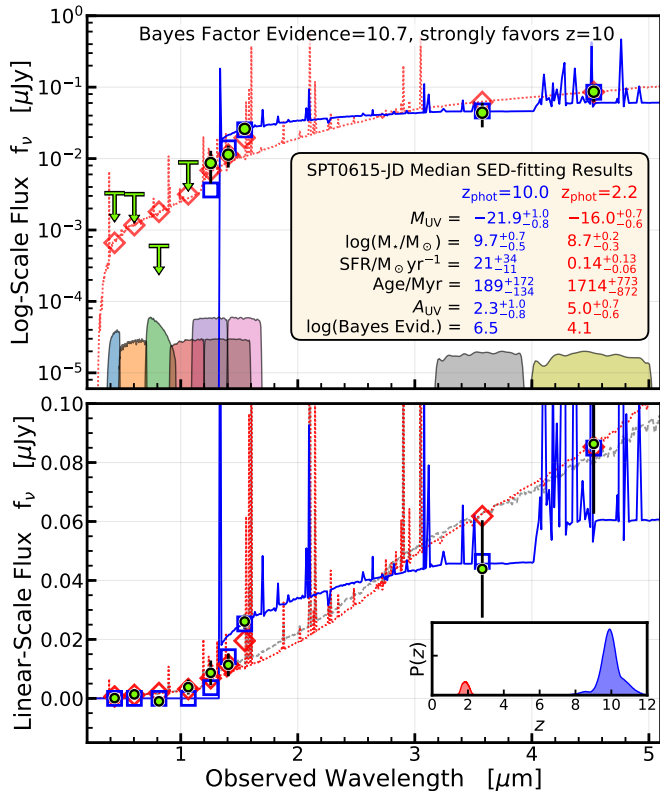


FIG. 2.— Best-fit SEDs to RELICS *HST* and *Spitzer* photometry (green circles) of SPT0615-JD. The solid blue line and squares (dotted red line and diamonds) show the best-fit SED and model fluxes respectively assuming the $z \sim 10$ ($z \sim 2$) solution. The top (bottom) plot displays the flux on a logarithmic (linear) scale, and the top plot also shows the *HST* and *Spitzer* transmission curves for reference. The dashed gray curve in the lower plot shows the $z \sim 2$ median SED. Fluxes have been corrected for lensing magnification ($\mu = 7$) and the *Spitzer* fluxes have not been adjusted despite likely contamination (see §2 and Fig. 1). The lower inset figure shows the redshift likelihood $P(z)$ which strongly favors the $z \sim 10$ solution. Though the $z \sim 2$ solutions formally have a $\sim 10\%$ likelihood, we argue they are unphysical in the text (§4).

the original arc, and therefore below the detection limit. All three models predict the lower-left counterimage to be of similar magnification and magnitude of the original arc, and LTM predicts the counterimages to have the same magnitude as the original arc. Given these models, we would have expected to see an image near the lower-left position, but none are yet detected. We note that the WFC3 limiting depths are ~ 26 AB mag, and the counterimages may be fainter. Conversely, all lens models predict no counterimages if SPT0615-JD is at $z \sim 2$. Deeper imaging of this field is required to properly search for the $z \sim 10$ counterimages and yield geometric support as in Coe et al. (2013), Zitrin et al. (2014), and Chan et al. (2017).

4. SED FITTING

Thanks to the *Spitzer* data that probes the rest-frame optical and near-ultraviolet (UV, $\sim 2900 - 4500$ Å), we can infer upper-limits on physical parameters like stellar mass and dust attenuation to test if the high and low-redshift solutions are sensible. We use a Bayesian SED-fitting procedure originally described by Papovich et al. (2001) and updated by Salmon et al. (2015). In short, we sample the posterior us-

ing a grid of SEDs that represent a range of stellar population ages ($10 \text{ Myr} < t_{\text{age}} < t_{\text{universe}}$, logarithmically spaced), attenuation ($0 < A_{\text{UV}} < 7.4$), metallicity ($0.02Z_{\odot} < Z < Z_{\odot}$), and rising star-formation histories ($\Psi(t) = \Psi_0 \exp(t/\tau_{\text{SFH}})$, where the e -folding timescale τ_{SFH} can be 0.3, 0.5, 0.7, 1, 3, 5, 7, 10, 30, 50, 70, or 100 Gyr). We use Bruzual & Charlot (2003) stellar population synthesis models with a Chabrier (2003) IMF³ and include the effects of nebular emission lines following Salmon et al. (2015). We assume the dust-attenuation law derived by Salmon et al. (2016) that varies in shape from a steep law at low attenuation (similar in shape to the extinction law of the Small Magellanic Cloud) to a grey law at high attenuation (similar in shape to the starburst curve of Calzetti et al. (2000)).

The results of our SED fitting are summarized in Fig. 2. For all SED fitting, we correct for lensing magnification assuming $\mu = 7$, and do not further correct the *Spitzer* fluxes despite likely contamination (see §2 and Fig. 1). The fits assuming the $z \sim 10$ redshift show a moderately high stellar mass of $M_{\star} = 10^{9.7^{+0.7}_{-0.5}} M_{\odot}$ and star-formation rate of $\text{SFR} = 21^{+34}_{-11} M_{\odot}/\text{yr}$. However, the stellar mass, star-formation rate, age, and UV dust attenuation will be lower if the rest-frame optical fluxes are over-estimated, as implied by the *Spitzer* contaminant shown in Fig. 1. Therefore, we consider these preliminary estimates to be upper limits. Nevertheless, the stellar mass and SFR of SPT0615-JD are indicative of a typical star-forming galaxy at $z \sim 10$ (Oesch et al. 2014) and would lie on the SFR- M_{\star} relation at $z \sim 6$ (Salmon et al. 2015).

The SED fit assuming $z \sim 2$ is quite different. The median, marginalized results, which account for the full probability density, imply a low stellar mass $M_{\star} = 10^{8.7^{+0.2}_{-0.3}} M_{\odot}$, low star-formation rate $\text{SFR} = 0.14^{+0.13}_{-0.06} M_{\odot}/\text{yr}$, and evolved stellar population age $t = 1714^{+773}_{-872}$ Myr, with high uncertainty. Similarly, the best-fit SED has the same stellar mass, but a higher SFR ($\text{SFR} \sim 3 M_{\odot}/\text{yr}$), a slightly younger stellar population age ($t = 1585$ Myr), a very dusty SED ($A_{\text{UV}} = 6.1$ mag), and high nebular emission ([OIII]+ H_{β} equivalent width $\text{EW} = 780$ Å, or 1671 Å to match the *H*-band magnitude).

This $z \sim 2$ SED solution is unphysical for several reasons. Its dust attenuation is dramatically high for its low stellar mass (Pannella et al. 2009), its size is too large and SED too dusty compared to other extreme [OIII] emitting galaxies at $z \sim 2$ (Malkan et al. 2017), and it has too high EW compared to [OIII] emitters at $z \sim 2$ of similar mass (Maseda et al. 2013). Such a rare high EW and high dust interloper was spectroscopically ruled out for a similar $z \sim 11$ candidate, MACS0646-JD (Pirzkal et al. 2015). Importantly, the $z \sim 2$ SED necessitates such strong [OIII] emission to match the observations with appreciable likelihood; a dusty SED template alone cannot match both the bright H-band flux and the relatively faint optical flux. Finally, unlike the $z \sim 10$ solution, the $z \sim 2$ solution requires the already overestimated *Spitzer* fluxes to be high, and it becomes increasingly harder to justify a $z \sim 2$ SED with lower $3.6 \mu\text{m}$ and $4.5 \mu\text{m}$ fluxes.

³ Switching from a Chabrier to a Salpeter (1955) IMF would result in higher derived stellar mass and star-formation rate (SFR) by 0.25 dex.

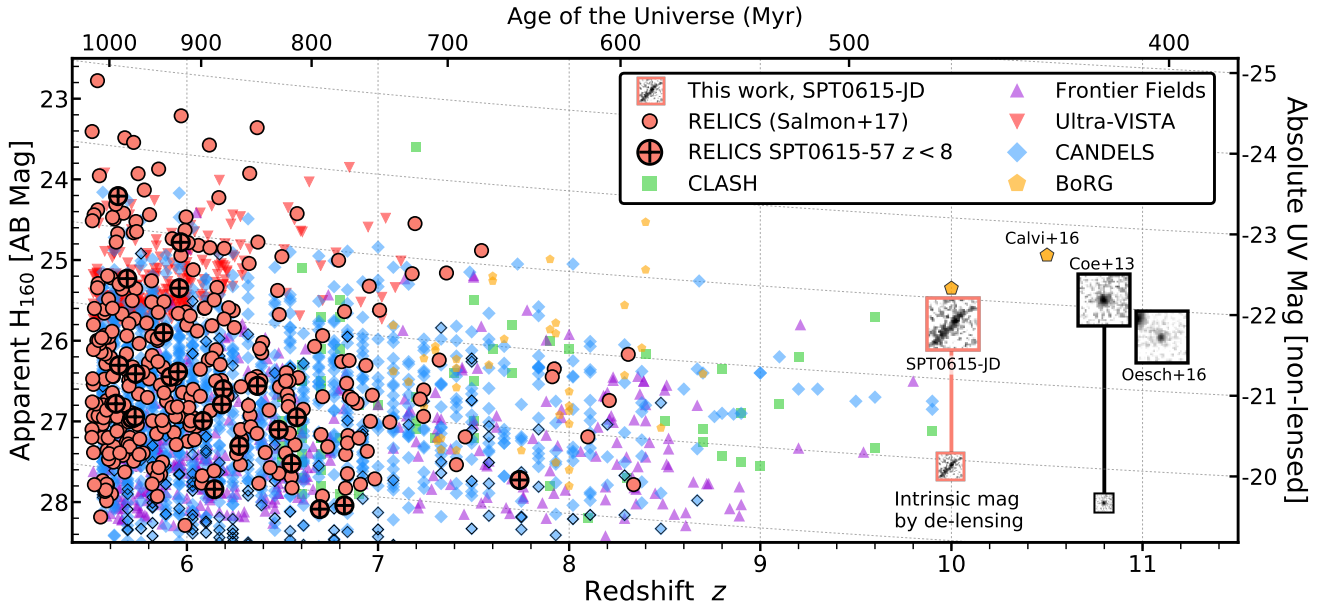


FIG. 3.— Observed H -band magnitude versus redshift for $z > 5.5$ candidates from various surveys. The $z < 8.5$ candidates from Salmon et al. (2017) are shown as salmon-colored circles, and the candidates from SPT0615-57 are filled with crosses. The green squares are galaxies from CLASH (Zheng et al. 2012; Bradley et al. 2014; Hoag et al. 2017), purple upwards-triangles from the Frontier Field (Zitrin et al. 2014; Ishigaki et al. 2017), red downwards-triangles from Ultra-VISTA (Bowler et al. 2017), blue diamonds from CANDELS (Bouwens et al. 2014, 2015; Oesch et al. 2016) (outlined diamonds are from the HUDF; see also Finkelstein et al. 2015), and orange pentagons from BoRG/HIPPIES (Bradley et al. 2012; Schmidt et al. 2014; Calvi et al. 2016). Gray lines follow the conversion from apparent to absolute UV magnitude to reference for un-lensed sources. $2'' \times 2''$ cutout images of two $z \sim 11$ candidates (Coe et al. 2013; Oesch et al. 2016) and the $z \sim 10$ candidate from this work mark their observed magnitudes respectively. For the latter two candidates, we also show their cutouts scaled in size according to their lens model to show an example of their intrinsic size (a full source-plane reconstruction of SPT0615-JD would show a smaller axis ratio). SPT0615-JD has a much larger observed size compared to the other candidates.

We caution the reader that the best-fit SEDs in Fig. 2 (and best-fit SED solutions in general) are not necessarily representative of the full probability density of the posterior (Leja et al. 2017). A better indicator of the goodness-of-fit than the best-fit χ^2 is the unconditional marginal likelihood of the data, or the Bayesian evidence (see e.g., Salmon et al. 2016, for definitions), which describes probability of seeing the data given all parameters. The ratio of two Bayesian evidences⁴ under different model assumptions, like whether we assume the SED lies at $z \sim 2$ or $z \sim 10$, is called the Bayes Factor and describes the relative evidence between two model assumptions. We find a Bayes-Factor evidence of 10.7 in favor of the $z \sim 10$ solution, which is considered “very strong” evidence (Kass & Raftery 1995). Our interpretation is that there are more SEDs that fit the data well assuming the $z \sim 10$ redshift than the select few (and justifiably unphysical) SEDs that fit the data well assuming the $z \sim 2$ redshift.

5. COMPARISON WITH OTHER HIGH-REDSHIFT CANDIDATES

Fig. 3 shows the H -band magnitude versus redshift for all high- z ($z > 5.5$) candidate galaxies discovered in RELICS (Salmon et al. 2017) and many other deep and wide surveys. The lensed, observed-frame size of SPT0615-JD stands out as spatially much larger than

other $z \sim 10$ candidates (other candidates at these redshifts have similar point-like sizes to those found by Coe et al. 2013 and Oesch et al. 2016, see below). The intrinsic (de-lensed) magnitude of SPT0615-JD is similar to that of the $z \sim 11$ candidate MACS0647-JD (Coe et al. 2013).

An independent way to test high and low- z solutions for SPT0615-JD is to calculate its physical size and compare to other known interlopers. Moreover, the sizes of galaxies can give us great physical insight into the initial conditions of early disk evolution (Ferguson et al. 2004). Broadly, the $z > 5$ size evolution at fixed luminosity scales as $(1+z)^{-m}$ where $m = 1-2$ (Shibuya et al. 2015). Holwerda et al. (2015) demonstrated that a combination of UV-to-optical color, sampled by the F160W and $3.6 \mu\text{m}$ bands, and physical size can be used to identify obvious low- z contaminants. They summarized that the sizes of $z > 9$ galaxy candidates have typical half-light radii of $r_e < 0.8$ kpc.

To calculate the size of SPT0615-JD, we used our lens models to reconstruct its image in the source plane. The LTM lens model finds a relatively mild tangential magnification, or shear, of a factor of ~ 3 , leaving the full width of the de-lensed source to be about 3–3.5 kpc. If we assume the light distribution is uniform, we can take the half light radius to be about $\sim 1/4$ of the full size and find $r_e \approx 0.7 - 0.8$ kpc. The statistical error on this size (from the lens model) is only a couple of percent, so we are dominated by systematic errors ($\sim 10\%$). Curiously, the reconstructed source’s axis ratio is still about 2:1 in the same direction as the lensing shear, which could mean that the shear is underestimated and the size is in fact

⁴ The Bayes-factor evidence is typically described as $\zeta = 2 \ln B_{12}$, where B_{12} is the ratio of the Bayesian evidence under model assumption 1 to that of model assumption 2. Larger positive numbers favor the assumptions in model 1, and negative favor the assumptions in model 2 (Kass & Raftery 1995).

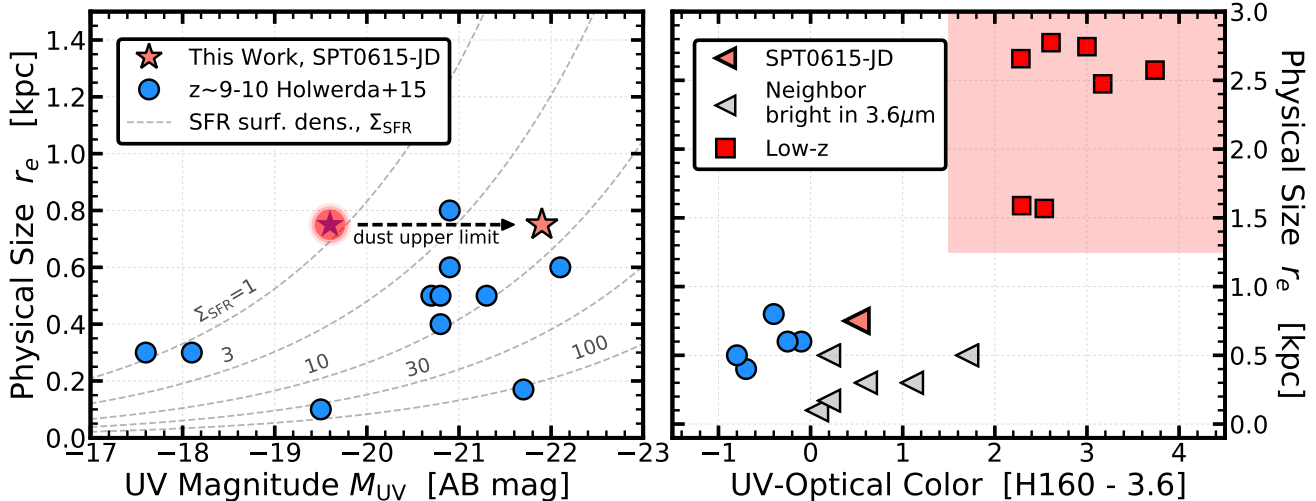


FIG. 4.— The size of SPT0615-JD compared to other known $z > 9$ galaxy candidates (blue circles). Left: the physical size (effective radius) as a function of absolute UV magnitude. The denedged magnitude is shown as the salmon-colored star, and the unobscured (corrected for our upper-limit dust extinction) denedged magnitude is shown as the salmon-colored star. Right: the physical size as a function of [F160W–3.6 μm] color. Triangles show $z > 9$ candidates, including SPT0615-JD (bold triangle), that may be contaminated in Spitzer flux by a bright neighbor, resulting in redder [F160W–3.6 μm] colors. Significantly larger sizes of typical very red $z \sim 2$ galaxies (red squares) are shown in the red box.

smaller.

Fig. 4 shows that the inferred size of SPT0615-JD is typical compared to other high- z candidates. This provides crucial evidence in support of the $z \sim 10$ solution that is independent of the galaxy SED. While the uncertainty in the $z \sim 10$ UV dust attenuation should be considered as an upper limit, the candidate is still within the range of M_{UV} and SFR surface density of known $z > 9$ candidates.

6. CONCLUSIONS

We present SPT0615-JD, a promising $z \sim 10$ galaxy candidate that appears to be stretched into the shape of an arc by the effects of strong gravitational lensing. Out of all combined lensing fields from RELICS, CLASH, and the Frontier Fields, there is no other galaxy candidate spatially stretched by lensing as distant as SPT0615-JD. While our three independent lens models predict at least one detectable counterimage, we do not see one in the current data. No counterimages are expected if the candidate is at lower redshift. However, the only $z \sim 2$ SED that fits the data well is unphysical based on the required combination of its size, mass, dust at-

tenuation, and [OIII]+H β EW. In addition, we find very strong Bayesian evidence that the SED-inferred physical properties of this candidate are of a $z \sim 10$ typical star-forming galaxy. Finally, the source-plane size of SPT0615-JD is similar to other $z = 9-10$ galaxies, while the observed-frame image offers unprecedented spatial resolution. This galaxy candidate offers the unique opportunity for resolving stellar populations deep in the epoch of reionization, especially with the higher resolution of *JWST*.

ACKNOWLEDGEMENTS

This paper uses observations from NASA/ESA *HST*. STScI is operated by AURA under NASA contract NAS 5- 26555. ACS under NASA contract NAS 5-32864, and *Spitzer* by JPL. These observations are associated with program GO-14096 and archival data with GO-9270, GO-12166, GO-12477, GO-12253. Some data were obtained from MAST. This work was performed under the auspices of the U.S. Department of Energy by LLNL under contract DE-AC52-07NA27344. F.A.-S. acknowledges support from Chandra grant G03-14131X.

REFERENCES

- Bertin, E., & Arnouts, S. 1996, *A&AS*, 117, 393
 Bouwens, R. J., Bradley, L., Zitrin, A., et al. 2014, *ApJ*, 795, 126
 Bouwens, R. J., Illingworth, G. D., Oesch, P. A., et al. 2015, *ApJ*, 803, 34
 Bowler, R. A. A., Dunlop, J. S., McLure, R. J., & McLeod, D. J. 2017, *MNRAS*, 466, 3612
 Bradley, L. D., Trenti, M., Oesch, P. A., et al. 2012, *ApJ*, 760, 108
 Bradley, L. D., Zitrin, A., Coe, D., et al. 2014, *ApJ*, 792, 76
 Bruzual, G., & Charlot, S. 2003, *MNRAS*, 344, 1000
 Calvi, V., Trenti, M., Stiavelli, M., et al. 2016, *ApJ*, 817, 120
 Calzetti, D., Armus, L., Bohlin, R. C., et al. 2000, *ApJ*, 533, 682
 Chabrier, G. 2003, *PASP*, 115, 763
 Chan, B. M. Y., Broadhurst, T., Lim, J., et al. 2017, *ApJ*, 835, 44
 Coe, D., Zitrin, A., Carrasco, M., et al. 2013, *ApJ*, 762, 32
 Ferguson, H. C., Dickinson, M., Giavalisco, M., et al. 2004, *ApJ*, 600, L107
 Finkelstein, S. L. 2016, *PASA*, 33, e037
 Finkelstein, S. L., Ryan, Jr., R. E., Papovich, C., et al. 2015, *ApJ*, 810, 71
 Hoag, A., Bradač, M., Trenti, M., et al. 2017, *Nature Astronomy*, 1, 0091
 Holwerda, B. W., Bouwens, R., Oesch, P., et al. 2015, *ApJ*, 808, 6
 Infante, L., Zheng, W., Laporte, N., et al. 2015, *ApJ*, 815, 18
 Ishigaki, M., Kawamata, R., Ouchi, M., Oguri, M., & Shimasaku, K. 2017, *ArXiv*, 1702.04867
 Jullo, E., Kneib, J.-P., Limousin, M., et al. 2007, *New Journal of Physics*, 9, 447
 Kass, R. E., & Raftery, A. E. 1995, *Journal of the American Statistical Association*, 90, 773
 Laporte, N., Ellis, R. S., Boone, F., et al. 2017, *ApJ*, 837, L21
 Leja, J., Johnson, B. D., Conroy, C., van Dokkum, P. G., & Byler, N. 2017, *ApJ*, 837, 170

- Mainali, R., Kollmeier, J. A., Stark, D. P., et al. 2017, *ApJ*, 836, L14
- Malkan, M. A., Cohen, D. P., Maruyama, M., et al. 2017, *ApJ*, 850, 5
- Maseda, M. V., van der Wel, A., da Cunha, E., et al. 2013, *ApJ*, 778, L22
- Merlin, E., Bourne, N., Castellano, M., et al. 2016, *A&A*, 595, A97
- Oesch, P. A., Bouwens, R. J., Illingworth, G. D., Labbe, I., & Stefanon, M. 2017, *ArXiv*, 1710.11131
- Oesch, P. A., Bouwens, R. J., Illingworth, G. D., et al. 2014, *ApJ*, 786, 108
- Oesch, P. A., Brammer, G., van Dokkum, P. G., et al. 2016, *ApJ*, 819, 129
- Oguri, M. 2010, *PASJ*, 62, 1017
- Pannella, M., Carilli, C. L., Daddi, E., et al. 2009, *ApJ*, 698, L116
- Papovich, C., Dickinson, M., & Ferguson, H. C. 2001, *ApJ*, 559, 620
- Pirzkal, N., Coe, D., Frye, B. L., et al. 2015, *ApJ*, 804, 11
- Planck Collaboration, Aghanim, N., Arnaud, M., et al. 2011, *A&A*, 536, A26
- Rigby, J. R., Bayliss, M. B., Gladders, M. D., et al. 2015, *ApJ*, 814, L6
- Salmon, B., Papovich, C., Finkelstein, S. L., et al. 2015, *ApJ*, 799, 183
- Salmon, B., Papovich, C., Long, J., et al. 2016, *ApJ*, 827, 20
- Salmon, B., Coe, D., Bradley, L., et al. 2017, *ArXiv*, 1710.08930
- Salpeter, E. E. 1955, *ApJ*, 121, 161
- Schmidt, K. B., Treu, T., Trenti, M., et al. 2014, *ApJ*, 786, 57
- Shibuya, T., Ouchi, M., & Harikane, Y. 2015, *ApJS*, 219, 15
- Smit, R., Swinbank, A. M., Massey, R., et al. 2017, *MNRAS*, 467, 3306
- Stark, D. P. 2016, *ARA&A*, 54, 761
- Stark, D. P., Richard, J., Siana, B., et al. 2014, *MNRAS*, 445, 3200
- Stark, D. P., Walth, G., Charlot, S., et al. 2015, *MNRAS*, 454, 1393
- Williamson, R., Benson, B. A., High, F. W., et al. 2011, *ApJ*, 738, 139
- Zheng, W., Postman, M., Zitrin, A., et al. 2012, *Nature*, 489, 406
- Zitrin, A., Zheng, W., Broadhurst, T., et al. 2014, *ApJ*, 793, L12
- Zitrin, A., Labbé, I., Belli, S., et al. 2015, *ApJ*, 810, L12